

Effect of an inhomogeneous external magnetic field on a quantum dot quantum computer

Rogerio de Sousa, Xuedong Hu, and S. Das Sarma

Department of Physics, University of Maryland, College Park, MD 20742-4111

(December 2, 2024)

We calculate the effect of an inhomogeneous magnetic field, which is invariably present in an experimental environment, on the exchange energy of a double quantum dot artificial molecule, projected to be used as a 2-qubit quantum gate in the proposed quantum dot quantum computer. We use two different theoretical methods to calculate the Hilbert space structure in the presence of the inhomogeneous field: the Heitler-London method which is carried out analytically and the molecular orbital method which is done computationally. Within these approximations we show that the exchange energy J changes slowly when the coupled dots are subject to a magnetic field with a wide range of inhomogeneity, suggesting swap operations can be performed in such an environment as long as quantum error correction is applied to account for the Zeeman term. We also point out the quantum interference nature of this slow variation in exchange.

I. INTRODUCTION

It has long been proposed that quantum mechanical computers might provide much more computing power than machines based on classical physics [1]. However, it was the discovery of fast quantum algorithms for tasks such as prime factorization and searching disordered databases [2] together with effective error correction schemes [3] that motivated a frenetic search for a suitable physical system on which reliable quantum hardware could be built.

Among the many proposed quantum hardware schemes the ion trap quantum computer, based on electronic states of laser cooled trapped ions, have not only demonstrated full control of elementary one and two-qubit (quantum bit, the basic unit of quantum information) logic gates but also recently produced 4-qubit entanglement [4]. Although the ion trap represents the current state of the art in quantum computing architecture, its scalability prospect is unclear, since moving a large number of ions between memory and computing sectors of the ion traps without destroying quantum coherence is a difficult problem. Another proposed scheme, the liquid state Nuclear Magnetic Resonance (NMR) quantum computer, based on nuclear spin states of molecules in solutions, recently demonstrated a 5-qubit order finding algorithm [5]. However, the NMR quantum computer also has a scalability problem, since the signal to noise ratio decreases exponentially as the size of the molecules increases. Furthermore, there has been a theoretical proof that no entanglement is present in the current ensemble-averaged NMR experiments [6], although its implication for NMR quantum computation has not yet been fully explored.

With the scalability problem in mind it has been suggested that advanced semiconductor technology might provide the basis for building a large (i.e. many qubits) quantum computer (QC), just as it has been proved to be effective in building today's classical digital computers. Two of the main proposals for such semiconductor QCs are based on qubits using the spin of a phosphorous donor nucleus in bulk silicon [7] and the spin of a single electron trapped in a GaAs quantum dot [8]. Even though our work here refers specifically to the latter, our results are valid for both solid state QC proposals since the two are similar in the sense that they use the same universal quantum gate to perform quantum computation: The exchange or swap gate which acts on two qubits coupled by an effective Heisenberg spin interaction and one-qubit gates that perform rotations on two orthogonal spin axes by applying external magnetic fields. Experimentally demonstrating the operation of any of these quantum gates is a formidable task and has not been carried out yet, and all semiconductor based QCs are at best promising proposals at this stage. Nevertheless, the hope is that after the first step of successfully demonstrating a single qubit in a semiconductor-based QC, scaling up from one qubit to many would be feasible based on the established infrastructure of semiconductor microelectronics industry. Moreover, precisely controlling the quantum dynamics of a few spins in a semiconductor nanostructure represents a major experimental challenge, and therefore any success will lead to new insight into mesoscopic spin properties of nanostructures, which by itself is a subject of intrinsic fundamental interest.

Quantum computation can be considered as a complicated unitary evolution of a N -qubit system, governed by a N -qubit Hamiltonian, where each qubit is a quantum mechanical two-level system. It has been proved that this usually extremely complicated process can be factored into a number (that is a polynomial in N) of simple one and two-qubit processes with sufficiently high accuracy, in analogy with a classical network of logic gates [9]. To improve efficiency multiple simple operations might be lumped together, as was proposed in various parallel pulse schemes [10]. In these operations for a quantum dot quantum computer (QDQC) an inhomogeneous magnetic field inevitably appears, as it is a powerful technique to rotate spins while controlling spin exchange. The inhomogeneity in the field

here arises necessarily from the fact that the parallel scheme employs local magnetic field pulses on individual dots to achieve different spin rotations, and a magnetic field localized on one dot is essentially an inhomogeneous field for a different dot. Furthermore, inhomogeneous magnetic fields can be produced by unwanted magnetic impurities or external currents in the sample, which will be invariably present in any real QDQC architecture. Since in the proposed parallel schemes the exchange coupling J (which controls the swap gate) is treated as independent of the magnetic field inhomogeneity [10], it is important to explore whether this dependence is truly weak enough, or if it is necessary to adjust the inter-dot barrier continuously in order to maintain the desired J in the presence of a varying inhomogeneous field (which will be a formidable, if not impossible, task).

We showed in a previous paper [11] that an inhomogeneous magnetic field leads to errors in the swap operation of two qubits because the Zeeman term in the effective Hamiltonian is not proportional to the total spin. For example, if we try to swap the state $|\uparrow\downarrow\rangle$ we would obtain $|\downarrow\uparrow\rangle$ plus an entangled component proportional to the magnetic field inhomogeneity. In other words, once a product state is entered, the output will always be entangled, although for practical purposes this error can be kept within the currently estimated error correction bounds ($\simeq 10^{-4}$) for usual field inhomogeneities. This result is based on the assumption that one knows J exactly in order to achieve the best control, otherwise there can be additional errors in swap because of the uncertainty in J .

Motivated by the above concerns and problems arising from inhomogeneous magnetic fields, we calculate in this paper the exchange coupling J of a two-electron double dot as a function of the inhomogeneity in the external magnetic field. We employ a single envelope function approach and calculate the orbital energies of the two electrons, thus relating the general two-electron problem to a special two-spin Hamiltonian, and analyze the effect of field inhomogeneities on the orbital degrees of freedom of the double dot structure. The current work is thus complementary to our recent publication [11] dealing with the field inhomogeneity induced errors in the swap operation.

Quite recently it has been demonstrated that QDQC can be done without any applied magnetic field as long as a price is paid in increasing the number of exchange operations: Two ($S = \frac{1}{2}, S_z = +\frac{1}{2}$) states of three spins are used as a qubit, and the nearest-neighbor exchange interaction can provide all the required one-qubit and two-qubit operations of a quantum computer [12]. In this scheme applications of external magnetic fields for single qubit operations is not required, as exchange gates provide both 1- and 2-qubit operations. This proposal removes the problem of having strong applied inhomogeneous fields. However, stray fields due to impurities and external currents can still be present, and must be taken into account using appropriate error corrections. In this paper we focus on clarifying the issues that arise in the simpler sequential scheme that may contain an applied inhomogeneous magnetic field as well as pointing out potential errors in all exchange QC schemes. Our results are also directly relevant to the proposed parallel pulse schemes as discussed above.

II. MODEL

We consider two electrons in a horizontally coupled GaAs double quantum dot structure [13,14] (Fig. 1). Since these electrons are at the bottom of the conduction band the single envelope function approach provides a sufficiently complete physical picture of their energy states. Suppose there is an inhomogeneous magnetic field applied so that the electron in the left well is subject to a field which is on average $2B_{dif}$ lower than the one in the right. For simplicity we assume a linearly changing field profile

$$\mathbf{B}(x, z) = (\overline{B} + B_{dif} \frac{x}{a_m}) \hat{\mathbf{z}} + B_{dif} \frac{z}{a_m} \hat{\mathbf{x}}, \quad (1)$$

where $\overline{B} = \frac{1}{2}(B_R + B_L)$, $B_{dif} = \frac{1}{2}(B_R - B_L)$, and $2a_m$ is the separation between the dots. The complete Hamiltonian is given by

$$H = H_{orb} + H_Z, \quad (2)$$

$$H_{orb} = h_1 + h_2 + C \quad (3)$$

$$h_i = \frac{1}{2m} \left(\mathbf{p}_i + \frac{e}{c} \mathbf{A} \right)^2 + V(\mathbf{x}_i), \quad (4)$$

$$C = \frac{e^2}{\varepsilon} \frac{1}{|\mathbf{x}_1 - \mathbf{x}_2|}, \quad (5)$$

$$H_Z = g^* \mu_B \sum_{i=1}^2 \mathbf{B}(\mathbf{x}_i) \cdot \mathbf{S}_i. \quad (6)$$

Here \mathbf{x}_i is the position of the i th electron in the xy plane, $m = 0.067m_e$ is the electron effective mass in GaAs, $\varepsilon = 13.1$ is the dielectric constant, $g^* = -0.44$ is the GaAs gyromagnetic ratio, and \mathbf{A} is the vector potential for the inhomogeneous field:

$$\mathbf{A} = - \left(\frac{\overline{B}}{2} y \right) \hat{\mathbf{x}} + \left[\frac{\overline{B}}{2} x + \frac{B_{dif}}{2a_m} (x^2 - z^2) \right] \hat{\mathbf{y}}. \quad (7)$$

Note that since the quantum dots are fabricated using a high mobility 2D electron gas (taken to be along the xy plane), the dot dynamics is assumed to be constrained to the $z = 0$ plane because the z-width of the 2D electron gas is typically much smaller than the QD confinement in the x-y plane. The z-dependent components in \mathbf{A} and \mathbf{B} do not have any effect other than to guarantee the $\nabla \times \mathbf{B} = \mathbf{0}$ condition. Hence the effect of $B_x = B_{dif}z/a_m$ will be neglected in our calculation (the 2D electron gas has a typical thickness of the order of a few nm and neglecting B_x is an excellent approximation for realistic QD systems). The confining potential V in the x-y plane is modeled in our calculations by a linear combination of gaussians characterized by the parameters V_0 , a , V_b , l_x , l_y , l_{bx} and l_{by} which can be adjusted to control the size of the dots and switch on and off the exchange coupling:

$$V = -V_0 \left[\exp \left(-\frac{(x-a)^2}{l_x^2} \right) + \exp \left(-\frac{(x+a)^2}{l_x^2} \right) \right] \exp \left(-\frac{y^2}{l_y^2} \right) + V_b \exp \left(-\frac{x^2}{l_{bx}^2} \right) \exp \left(-\frac{y^2}{l_{by}^2} \right). \quad (8)$$

In our calculation we choose $V_0 = 50\text{meV}$ as the potential well depth and $V_b = 30\text{meV}$ as the central barrier height. In addition, $a = 15\text{nm}$, $l_x = l_y = 30\text{nm}$, $l_{bx} = 15\text{nm}$, and $l_{by} = 80\text{nm}$, which leads to an effective barrier height (difference in energy between the top of the central barrier and the bottom of one of the wells) of 9.65meV , and a slightly shifted potential minimum $a_m = 16.41\text{nm}$. We note that our choice of Eq. (8) as the QD confinement potential model is actually quite a general approximation, and allows considerable flexibility in our QDQC Hilbert space structure calculations.

An important feature of the Zeeman Hamiltonian (6) is that it couples coordinate \mathbf{x}_i with spin \mathbf{S}_i in an inhomogeneous field. This interaction introduces a coupling between the singlet and the $S_z = 0$ triplet state, and can be well described (in the Heitler-London approximation) by an effective spin Hamiltonian [11]

$$H_Z \cong \gamma_R S_{1z} + \gamma_L S_{2z}, \quad \gamma_R = g^* \mu_B B_R, \quad \gamma_L = g^* \mu_B B_L. \quad (9)$$

But note that Eq. (9) is not invariant under particle permutation P_{12} , which is a natural consequence of the fact that it has a non-vanishing matrix element between singlet and triplet states (which are respectively odd and even under a P_{12} operation acting only in the two-spin space). This lifting of the permutation symmetry is a direct consequence of the inhomogeneous external magnetic field in this problem.

Our main objective is to study the dependence of the exchange coupling J on the inhomogeneity of the magnetic field. The parameter J describes the splitting between the lowest energy singlet and triplet states of the Hamiltonian (2), which at low energy reduces to the effective two-spin Heisenberg-type Hamiltonian that enables the operation of the quantum gates,

$$H_{eff} = J \mathbf{S}_1 \cdot \mathbf{S}_2 + \gamma_R S_{1z} + \gamma_L S_{2z}. \quad (10)$$

We use four different approximations to calculate J from the orbital Hamiltonian given in Eq. (3): Heitler-London (HL), Molecular Orbital with S states (MO-S), with up to P states (MO-SP), and with up to D states (MO-SPD). It should be noted that the Zeeman splitting term given in Eq. (9) does not affect the calculation of J in any way and it is only added to Eq. (10) after J has been determined in order to obtain the effective 2-spin exchange Hamiltonian controlling the quantum gates.

III. METHODS AND RESULTS

To diagonalize the Hamiltonian given in Eq. (3), we use as our one particle basis the so called Fock-Darwin energy states centered at the bottom of the left and right wells ($x = \pm a_m$, $y = 0$). The Fock-Darwin QD states, briefly described in Appendix A of this paper for the sake of completeness and notational clarity, are simply the quantized states of the 2D orbital motion of the electrons in the presence of an external parabolic confinement potential and

magnetic field. Fock-Darwin states have a principal quantum number n which describes a shell structure: $n=0$ is referred to as S states, $n=1$ as P, $n=2$ as D, and so on. Each shell is composed of $n+1$ levels labeled by the magnetic quantum number $m=-n, -n+2, \dots, n-2, n$. Their energy is given by $E_{nm}^{R/L} = \hbar\Omega^{R/L}(n+1) + \frac{1}{2}\hbar\omega_c^{R/L}m$ where $\Omega^{R/L} = \sqrt{\omega_0^2 + (\omega_c^{R/L}/2)^2}$, $\omega_c^{R/L} = eB_{R/L}/mc$ is the cyclotron frequency and $\omega_0 = \sqrt{V_0/ml_x^2}$ approximates the harmonic confinement frequency near the bottom of the dot potential. Each Fock-Darwin state has a characteristic width $l_{0R/L} = \sqrt{\hbar/m\Omega^{R/L}}$, which assumes different values depending on whether the state is in the right well subject to a field B_R or in the left well where the field is B_L , which are different in the inhomogeneous field case we are studying. Notice that the vector potential (7) is centered in between the dots which is located $\pm a_m$ to the side of each well. This means that we have to use basis functions which are gauge transformed Fock-Darwin states with an additional magnetic phase $\exp\left(\pm i\frac{eB_{L/R}a_m y}{2\hbar c}\right)$ (sign + and - refer to the left and right wells respectively).

In what follows we use this Fock-Darwin single electron basis to form two-electron states and solve our two-particle problem in two approximations: Heitler-London which can be solved analytically and Molecular Orbital which is solved numerically.

A. Heitler-London

Heitler-London (HL) is the simplest method to calculate the exchange coupling J in two coupled dots. It consists of the singlet and triplet wave functions formed from the lowest Fock-Darwin states ($n=m=0$):

$$\Psi_{S/T}(1, 2) = \frac{1}{\sqrt{2(1 \pm |S|^2)}} (\Psi_L(1)\Psi_R(2) \pm \Psi_R(1)\Psi_L(2)) \chi_{s/t}, \quad (11)$$

$$\Psi_{R/L}(\mathbf{r}) = \frac{1}{\sqrt{\pi}l_{0R/L}} \exp\left(-\frac{(x \mp a_m)^2 + y^2}{2l_{0R/L}^2}\right) \exp\left(\mp i\frac{eB_{R/L}a_m y}{2\hbar c}\right), \quad (12)$$

where the spin functions are $\chi_s = \frac{1}{\sqrt{2}}(|\uparrow\downarrow\rangle - |\downarrow\uparrow\rangle)$ and χ_t is one of the three triplet states $\frac{1}{\sqrt{2}}(|\uparrow\downarrow\rangle + |\downarrow\uparrow\rangle, |\uparrow\uparrow\rangle, |\downarrow\downarrow\rangle)$. The exchange energy is then calculated as the difference between the expectation values of the Hamiltonian (3) calculated with the singlet and triplet trial wave functions:

$$J = \langle T | H_{orb} | T \rangle - \langle S | H_{orb} | S \rangle. \quad (13)$$

Using this formula in an inhomogeneous field, we can obtain an exact expression for J , which is quite complicated when both \bar{B} and B_{dif} are nonzero, and is given in its entirety in Appendix B. Here we show the expression for J in the special situation when $\bar{B} = 0$, which catches the main qualitative features of the inhomogeneous case:

$$\begin{aligned} J(\bar{B} = 0, B_{dif}) = & \frac{2S^2}{1 - S^4} \left\{ \frac{\hbar^2 a_m^2}{ml_0^4} + \frac{1}{4} \frac{e^2}{mc^2} B_{dif}^2 (3l_0^2 - a_m^2) - \frac{2V_0 l_x l_y}{\sqrt{(l_x^2 + l_0^2)(l_y^2 + l_0^2)}} \right. \\ & \times \left[\exp\left(-\frac{(a - a_m)^2}{l_x^2 + l_0^2}\right) + \exp\left(-\frac{(a + a_m)^2}{l_x^2 + l_0^2}\right) - 2 \exp\left(-\frac{a^2}{l_x^2 + l_0^2}\right) \right] \\ & \left. - \frac{2V_b l_{bx} l_{by}}{\sqrt{(l_{bx}^2 + l_0^2)(l_{by}^2 + l_0^2)}} \left[1 - \exp\left(-\frac{a_m^2}{l_{bx}^2 + l_0^2}\right) \right] - \sqrt{\frac{\pi}{2}} \frac{e^2}{\varepsilon l_0} \left[1 - SI_0\left(\frac{a_m^2}{l_0^2}\right) \right] \right\}, \end{aligned} \quad (14)$$

where $S = \exp(-a_m^2/l_0^2)$ is the overlap, $l_0 = l_{0R} = l_{0L}$ the Fock-Darwin characteristic width (the same for the left and right wells in the $\bar{B} = 0$ case as $|B_L| = |B_R|$), and I_0 the zeroth order modified Bessel function. Note that in general $a_m \neq a$ since the location of the minimum in the wells is usually different from the parameter $a = 15nm$. The main difference between Eq. (14) and the homogeneous field $B_{dif} = 0, \bar{B} \neq 0$ case (see Appendix B) is that the latter contains a number of phase interference terms proportional to $\exp[-(e\bar{B}/2\hbar c)^2 a_m^2 l_0^2]$, responsible for the faster decay of J as a function of \bar{B} as will be discussed below. In Fig. 2 we depict, primarily for the purpose of comparison with the inhomogeneous field results shown in Figs. 3 and 4, the calculated exchange coupling J as a function of the external magnetic field B in the homogeneous field case with $B_{dif} = 0$ in all our approximations.

Two curves calculated for different inhomogeneities using the HL approximation are shown in Fig. 3. The HL method is qualitatively reasonable, however, quantitatively it differs significantly from the more sophisticated molecular orbital calculations described below in section III B because J depends sensitively on the wave function overlap, which can be significantly affected by including higher excited states (as is done in MO calculations, but neglected in the HL theory). Even though the maximum field gradient obtainable in a laboratory is around 1 T in a 30nm range, we show values of B_{dif} that go all the way up to 5 T for completeness.

B. Molecular orbital calculation

The basic idea of the MO calculation is to mix in higher excited states in the set of basis states so as to improve the energetics. To go beyond the HL approximation, we can assemble more two-particle wave functions from the Fock-Darwin states, which we call molecular orbitals

$$\Psi_i(1, 2) = \frac{1}{\sqrt{2}} (\Psi_{i(1)}(1)\Psi_{i(2)}(2) \pm \Psi_{i(2)}(1)\Psi_{i(1)}(2)) \chi_{s/t} . \quad (15)$$

Electrons are fermions so the singlet has to be symmetric in space while the triplet is antisymmetric. Here we use this molecular orbital (MO) basis to solve a generalized eigenvalue problem $\mathbf{H} \cdot \Psi = E \mathbf{S} \cdot \Psi$ where $H_{ij} = \langle \Psi_i | H | \Psi_j \rangle$, $\Psi = (\Psi_1, \Psi_2, \dots)$ is the vector state and the overlap matrix $S_{ij} = \langle \Psi_i | \Psi_j \rangle$ is needed for orthonormalization since the MO basis is in general not orthonormal. We have done such a calculation in a constant homogeneous field [14], using both S and P Fock-Darwin states. Here we perform calculations with the progressively larger basis sets of S, SP, and SPD states in the inhomogeneous field problem.

In the simplest MO calculation we use only the Fock-Darwin S states to form the two-electron orbitals. Such a calculation improves upon the HL method by incorporating the doubly occupied states $\Psi_R(1)\Psi_R(2)$ and $\Psi_L(1)\Psi_L(2)$ and we call this the MO-S calculation. We then have a 3×3 singlet matrix to diagonalize, and the triplet energy is the same as the HL case (a 1×1 matrix). Note that we cannot use parity symmetry here to break up the matrices in a block diagonal form as was done before [14] since the field is inhomogeneous in the x direction. The resulting MO calculation is carried out numerically. The results of such calculations are shown in Figures 2 (homogeneous case), and 3 (inhomogeneous case) where there is a noticeable quantitative difference between the HL and MO-S exchange energies.

To improve the accuracy of our molecular orbital calculations, we also perform an MO-SP calculation, adding to our basis the $n = 1$, $m = \pm 1$ states on each side so that we have 6 one particle levels in total. The singlet MO-SP matrix is 21×21 ($\binom{6}{2} + 6 = 21$) and the triplet matrix is 15×15 . We are able to efficiently calculate the Coulomb matrix elements $C_{ij} = \langle \Psi_i | C | \Psi_j \rangle$ by reducing the 4-dimensional two-particle integrals to a 1D integral using the identity

$$\frac{1}{|\mathbf{x}_1 - \mathbf{x}_2|} = \frac{1}{r_{12}} = \frac{1}{\sqrt{\pi}} \int_0^\infty \frac{ds}{\sqrt{s}} \exp(-sr_{12}^2) \quad (16)$$

and integrating over \mathbf{x}_1 and \mathbf{x}_2 in the gaussian basis [15]. We then further increase the size of the MO basis by including Fock-Darwin D states ($n=2$, $m=-2,0,2$). We now have 12 single-particle levels, leading to a 78×78 and a 66×66 two-electron Hamiltonian matrix in the singlet and triplet basis, respectively.

Before we analyze our results it is important to determine the range of validity of our approximations. A strong inhomogeneity across the region where our basis functions vary appreciably leads to the necessity of including more and more orbitals to calculate the energy levels accurately. The extra terms that a non-vanishing inhomogeneity ($B_{dif} \neq 0$) adds to the one particle Hamiltonian can be written explicitly as a one particle operator ΔH . We write the vector potential as $\mathbf{A} = \mathbf{A}_R + \delta_R$ where δ_R represents the deviation from $\mathbf{A}_R = -\frac{1}{2}yB_R\hat{\mathbf{x}} + \frac{1}{2}xB_R\hat{\mathbf{y}}$ which describes the field in the right well. The one particle Hamiltonian becomes

$$h_i = \frac{1}{2m} \left(\mathbf{p}_i + \frac{e}{c} \mathbf{A}_R \right)^2 + V + \underbrace{\frac{e}{mc} \delta_R \cdot \left(\mathbf{p}_i + \frac{e}{c} \mathbf{A}_R \right) + \frac{1}{2m} \left(\frac{e}{c} \right)^2 \delta_R^2}_{\Delta H} . \quad (17)$$

ΔH is the part of the orbital Hamiltonian (3) that is most sensitive to inhomogeneities in the magnetic field, since it is proportional to B_{dif}^2 . In an inhomogeneous field, it strongly couples the S orbitals with the P and D orbitals, as can be seen from Table 1, where this orbital mixing is quantitatively represented. Each individual term in ΔH contributes approximately the same to the coupling, so we cannot neglect any of the terms in the calculation.

Note that as B_{dif} increases, the corrections to the MO energy levels grows very fast, reaching 10% of the exchange coupling J ($J \cong 0.2\text{meV}$ at $\overline{B} = 0T$ and $J \cong 0.1\text{meV}$ at $\overline{B} = 4T$) for $B_{dif} \cong 1T$ in the second and third columns of Table 1. This suggests that the HL, MO-S and MO-SP approximations are only reliable up to $B_{dif} = 1T$ for both the $\overline{B} = 0T$ and $\overline{B} = 4T$ cases. Moreover, a good estimate for the reliability of our best approximation, MO-SPD can be set as $B_{dif} = 4T$ for the $\overline{B} = 0T$ case and $B_{dif} = 2T$ for the $\overline{B} = 4T$ case. In Fig. 3 we show the exchange coupling J calculated only up to $B_{dif} = 5T$, which is an upper limit on the reliability of all our approximations. For completeness, Fig. 4 displays the same J calculated up to $B_{dif} = 25T$ (In this context, we should emphasize that in realistic experimental situations B_{dif} is likely to be much less than 1 T).

On the other hand, our approximations are increasingly better at low inhomogeneity, as can be seen in Table I. Fig. 3 shows that the exchange coupling J decreases only by 0.1% in the $\overline{B} = 0T$ case when $B_{dif} = 0.5T$, which is the maximum field gradient obtainable in an experiment ($\partial B_z / \partial x \cong 300\text{Gauss/nm}$). Also, in the $\overline{B} = 4T$ case it increases by 0.6% when the same field gradient is present. Using these values we can estimate that the error correction upper bound (10^{-4}) corresponds to an inhomogeneity of 30Gauss/nm . In section IV below we will argue that quantum interference in the inhomogeneous case is responsible for such a small change in J , as contrasted with the homogeneous situation in Fig. 2. Moreover, Fig. 3b shows that the exchange coupling J slightly increases as we switch on the inhomogeneity in a finite field ($\overline{B} = 4T$). All our approximations yield an increasing J , which can be understood in a simple one-particle picture. As we increase B_{dif} the magnetic field on the right (B_R) also increases, squeezing the Fock-Darwin state located on the right quantum dot. However, the left magnetic field (B_L) decreases to less than 4 T, which leads to a broad electronic wave function on the left quantum dot. When $B_{dif} = 4T$, the electronic state on the left dot reaches its maximum width, and starts to be squeezed for greater inhomogeneities. This suggests a maximum of the exchange coupling J located around $B_{dif} = 4T$. This maximum is not evident in our approximations simply because they lose their accuracy for B_{dif} below 4 T as discussed above, but an increasing trend in J is apparent from Fig. 3b. Moreover, by looking at the $\overline{B} = 0T$ case (Fig. 3a) we can infer that J is probably not increasing, since, as the MO approximations becomes more accurate, J first increase (MO-S and MO-P) and then decreases (MO-SPD). No maximum in J is expected here since as B_{dif} increases both the left and right electrons are squeezed.

IV. DISCUSSION

Comparing the results presented in Figs. 2 and 3 it becomes evident that J decreases much faster (Fig. 2) in the homogeneous magnetic field, even becoming negative at around 5T, in both HL and MO approximation schemes. This behavior can be roughly understood as arising from the approximate proportionality of J to the wave function overlap $S = \int \Psi_R^* \Psi_L d\mathbf{r}$ ($\Psi_{R/L}$ are defined in Eq. (12)) multiplied by a polynomial in \overline{B} and B_{dif} which explains features such as the singlet-triplet crossing in Fig. 2 (the overlap S is plotted in dimensionless units together with our results for J). It turns out that S is very sensitive to the magnetic phase $\exp\left(\pm i \frac{eB_{L/R}a_m y}{2\hbar c}\right)$ which appears in the right and left basis functions discussed above. In a homogeneous field, $B_R = B_L = B$ and those phases add up to give an extra exponential decay proportional to B^2 in the overlap: $S_{Hom} = \exp\left(-(a_m/l_0)^2\right) \exp\left(-\left(\frac{1}{2}l_0a_m\frac{eB}{\hbar c}\right)^2\right)$. On the other hand in the inhomogeneous case with $\overline{B} = 0$, $B_R = -B_L$ the phases cancel out in the S integral leaving just a single exponential decay, $S_{Inh} = \exp\left(-(a_m/l_0)^2\right)$ which depends mainly on the interdot distance. This absence of quantum interference in the inhomogeneous field case explains why J hardly changes when there is a magnetic field difference over the two quantum dots (Fig. 3), which is in fact good news for the operation of the swap gate in an environment that contains some magnetic impurities for example (or a field inhomogeneity arising from some other unintended source).

Note that in the homogeneous case the exchange coupling constant in Fig. 2 decreases extremely strongly at a few Tesla which leads to a singlet-triplet crossing. This crossing arises from the competition between the long range Coulomb interaction (which favors the triplet state) and the kinetic energy (favoring the singlet state). There is no such singlet-triplet crossing in an inhomogeneous field (except when \overline{B} is such that $J < 0$, where the application of B_{dif} leads to a positive J), because the kinetic energy term (which favors the singlet state) now dominates as quantum interference terms are suppressed. In the homogeneous field case on the other hand the potential energy term always wins at high enough B fields leading to the triplet state becoming lower in energy than the singlet state.

V. CONCLUSION

In conclusion, we study the singlet-triplet splitting (i.e. the exchange coupling) J of a horizontally coupled double quantum dot system with two electrons. In particular, we calculate J when the magnetic field is inhomogeneous with different field strengths ($\Delta B = 2B_{dif}$) in each dot, and show that realistic values of field inhomogeneity in double quantum dot structures should have quantitatively small (but qualitatively interesting) effect on J . We perform an analytical Heitler-London calculation, and a numerical diagonalization of the orbital Hamiltonian in a set of increasingly larger two-electron MO basis to conclude that the cancellation of the magnetic phase difference between the two electrons on the dots is responsible for the relatively weak dependence of J on B_{dif} for realistic values of B_{dif} . The swap gate can thus be operated in an inhomogeneous environment as long as the exchange coupling J is properly chosen and quantum error correction is performed to account for the inhomogeneity-induced errors arising from the Zeeman term as discussed earlier [11]. We conclude therefore that electron spin based QDQC operations should in principle be feasible in an inhomogeneous magnetic field environment (with the inhomogeneity arising either from external magnetic fields needed for single qubit manipulation, or for running the parallel pulse scheme or from unintended magnetic impurities or currents invariably present in the system) as long as the field inhomogeneity is not too large.

This work is supported by ARDA and the US-ONR. RdS acknowledges useful discussions with Dr. J. Fabian.

APPENDIX A: FOCK-DARWIN STATES

We briefly describe the Fock-Darwin states [16], which are used as the single particle basis in our calculations. Consider an electron of mass m^* restricted to move in the x-y plane and confined in a parabolic well of frequency ω_0 . A magnetic field B is applied in the z direction, which can be described by the vector potential $\mathbf{A} = -\frac{1}{2}yB\hat{\mathbf{x}} + \frac{1}{2}xB\hat{\mathbf{y}}$. The Hamiltonian then becomes

$$H = \frac{1}{2m^*} \left(\mathbf{p} + \frac{e}{c} \mathbf{A} \right)^2 + \frac{1}{2}m^*\omega_0^2 r^2, \quad (\text{A1})$$

where $r = \sqrt{x^2 + y^2}$ is the distance between the electron and the origin, e the electronic charge and c the speed of light. Since this Hamiltonian commutes with the z component of the angular momentum operator L_z , its eigenfunctions can be chosen with well defined angular momentum $m\hbar$. Apart from the magnetic quantum number m , a radial quantum number n completely describes the eigenenergies of the system, given by $E_{nm} = (n+1)\hbar\Omega + \frac{1}{2}m\hbar\omega_c$, with $n = 0, 1, 2, \dots$ and $m = -n, -n+2, \dots, n-2, n$. Here $\omega_c = \frac{eB}{m^*c}$ is the electron's cyclotron frequency whereas $\Omega = \sqrt{\omega_0^2 + (\omega_c/2)^2}$ is the harmonic oscillator frequency renormalized by the magnetic field. For small magnetic fields ($\omega_c \ll \omega_0$) the quantum number n describes a shell structure, with $n = 0, 1, 2, \dots$ being the S, P, D, \dots shells respectively. In table 2 below we write the angular momentum and energy eigenfunctions for the S, P and D shells that are used in calculations throughout this paper. The negative m wave functions can be easily obtained from the positive ones using the relation $\phi_{n-m}(r, \theta) = \phi_{nm}^*(r, \theta)$. Note that a characteristic length $l_0 = \sqrt{\hbar/m\Omega}$ sets the range of these wave functions.

APPENDIX B: EXCHANGE COUPLING J IN THE HEITLER-LONDON APPROXIMATION

Here we write down our analytical results in our calculation of the exchange coupling J in the Heitler-London approximation. \overline{B} and B_{dif} define the inhomogeneous external magnetic field in the system (Fig. 1). As described in section III A, J is calculated by subtracting the average energies of the Heitler-London states $\Psi_{S/T}$ (Eq. (11)) leading to

$$J = \frac{2}{1 - |S|^4} \left\{ |S|^2 [\langle \Psi_R | h | \Psi_R \rangle + \langle \Psi_L | h | \Psi_L \rangle + D] - [2\text{Re}(S\langle \Psi_R | h | \Psi_L \rangle) + I] \right\}, \quad (\text{B1})$$

where h is the single particle Hamiltonian (3), and $S = \langle \Psi_L | \Psi_R \rangle$ is the overlap. We also define the direct (D) and exchange (I) Coulomb integrals

$$D = \int |\Psi_L(1)|^2 \frac{e^2/\varepsilon}{|\mathbf{x}_1 - \mathbf{x}_2|} |\Psi_R(2)|^2 d\mathbf{x}_1 d\mathbf{x}_2, \quad (\text{B2})$$

$$I = \int \Psi_L^*(1) \Psi_R^*(2) \frac{e^2/\varepsilon}{|\mathbf{x}_1 - \mathbf{x}_2|} \Psi_L(2) \Psi_R(1) d\mathbf{x}_1 d\mathbf{x}_2, \quad (\text{B3})$$

where e is the electron charge and ε the dielectric constant of the material. We list below all the analytic expressions for those quantities as a function of the effective mass m , the characteristic lengths in the right and left wells $l_{0R/L} = \sqrt{\hbar/m\Omega^{R/L}}$, the magnetic fields $B_{R/L} = \bar{B} \pm B_{dif}$, and the confining potential parameters $a, l_x, l_y, l_{bx}, l_{by}$ (Eq. (8)). Note that a_m is the minimum location of each well, which is in general different than the parameter a . Throughout the expressions we use the zeroth order modified Bessel function $I_0(x)$, $\gamma = \frac{1}{l_{0R}^2} + \frac{1}{l_{0L}^2}$, $\lambda = \frac{1}{l_{0R}^2} - \frac{1}{l_{0L}^2}$, $b = \frac{e\bar{B}}{\hbar c}$, and the overlap S , which are listed below.

$$S = \frac{2l_{0R}l_{0L}}{l_{0L}^2 + l_{0R}^2} \exp\left(-\frac{2a_m^2}{l_{0L}^2 + l_{0R}^2} - \frac{b^2a_m^2}{2\gamma}\right), \quad (\text{B4})$$

$$D = \sqrt{\pi} \frac{e^2}{\varepsilon} \frac{1}{\sqrt{l_{0L}^2 + l_{0R}^2}} \exp\left(-\frac{2a_m^2}{l_{0L}^2 + l_{0R}^2}\right) I_0\left(\frac{2a_m^2}{l_{0L}^2 + l_{0R}^2}\right), \quad (\text{B5})$$

$$I = \sqrt{\pi} \frac{e^2}{\varepsilon} \frac{S}{\sqrt{l_{0L}^2 + l_{0R}^2}} \exp\left(-\frac{2a_m^2}{l_{0L}^2 + l_{0R}^2}\right) I_0\left(\frac{b^2a_m^2}{2\gamma}\right), \quad (\text{B6})$$

$$\begin{aligned} \langle \Psi_L | h | \Psi_L \rangle = & \frac{\hbar^2}{2ml_{0L}^2} + \frac{1}{8} \frac{e^2}{mc^2} \left[\bar{B}^2 - (B_R - B_L)B_L + \frac{3}{4} \frac{l_{0L}^2}{a_m^2} B_{dif}^2 \right] l_{0L}^2 \\ & - \frac{V_0 l_x l_y}{\sqrt{(l_{0L}^2 + l_x^2)(l_{0L}^2 + l_y^2)}} \left[\exp\left(-\frac{(a_m + a)^2}{l_{0L}^2 + l_x^2}\right) + \exp\left(-\frac{(a_m - a)^2}{l_{0L}^2 + l_x^2}\right) \right] \\ & + \frac{V_b l_{bx} l_{by}}{\sqrt{(l_{0L}^2 + l_{bx}^2)(l_{0L}^2 + l_{by}^2)}} \exp\left(-\frac{a_m^2}{l_{0L}^2 + l_{bx}^2}\right). \end{aligned} \quad (\text{B7})$$

For the average of the single particle Hamiltonian h in the right side, just substitute L for R and vice-versa in the expression above.

$$\begin{aligned} \langle \Psi_R | h | \Psi_L \rangle = & \frac{1}{2\gamma} S \left\{ -\frac{\hbar^2}{m} \frac{1}{l_{0L}^2 l_{0R}^2} \left(\frac{4a_m^2}{l_{0L}^2 + l_{0R}^2} - 2 \right) + \frac{e^2 a_m^2}{mc^2} \left[\frac{\gamma}{4} (\bar{B}^2 + B_{dif}^2) - \frac{\bar{B}^2}{l_{0L}^2 + l_{0R}^2} - \frac{\lambda}{2} \bar{B} B_{dif} \right] \right. \\ & + \frac{2}{\gamma} \frac{e^2 a_m^2}{mc^2} \left[\frac{\bar{B}^2}{l_{0L}^2 l_{0R}^2} + \frac{1}{4} \left(\lambda \bar{B} + \frac{B_{dif}}{a_m^2} + \frac{\lambda^2}{\gamma} B_{dif} \right) (\lambda \bar{B} - \gamma B_{dif}) \right] \\ & + \frac{1}{4} \frac{e^2 \bar{B}^2}{mc^2} \left[2 - \frac{b^2 a_m^2}{\gamma} + \frac{3}{\gamma a_m^2} \left(\frac{B_{dif}}{\bar{B}} \right)^2 + \frac{\lambda}{\gamma} \left(1 + \frac{\lambda}{\gamma} \frac{B_{dif}}{\bar{B}} \right) \left(\lambda a_m^2 + \frac{B_{dif}}{\bar{B}} \left(\frac{\lambda^2}{\gamma} a_m^2 + 6 \right) \right) \right] \\ & - \frac{V_0}{\sqrt{\frac{1}{2} \left(1 + \frac{l_{0L}^2}{l_{0R}^2} \right) + \frac{l_{0L}^2}{l_y^2}} \sqrt{\frac{1}{2} \left(1 + \frac{l_{0R}^2}{l_{0L}^2} \right) + \frac{l_{0R}^2}{l_x^2}}} \exp\left(-\frac{b^2 l_x^2 a_m^2}{2(2 + \gamma l_x^2)} - \frac{2l_x^2 a_m^2}{l_{0L}^2 l_{0R}^2 (2 + \gamma l_x^2)}\right) \\ & \times \left[\exp\left(-\frac{(a_m - a)^2 / l_{0R}^2 + (a_m + a)^2 / l_{0L}^2}{2 + \gamma l_x^2}\right) + \exp\left(-\frac{(a_m - a)^2 / l_{0L}^2 + (a_m + a)^2 / l_{0R}^2}{2 + \gamma l_x^2}\right) \right] \\ & \left. + \frac{V_b}{\sqrt{\frac{1}{2} \left(1 + \frac{l_{0L}^2}{l_{0R}^2} \right) + \frac{l_{0L}^2}{l_{by}^2}} \sqrt{\frac{1}{2} \left(1 + \frac{l_{0R}^2}{l_{0L}^2} \right) + \frac{l_{0R}^2}{l_{bx}^2}}} \exp\left(-\frac{b^2 l_{by}^2 a_m^2}{2(2 + \gamma l_{by}^2)} - \frac{2 \frac{l_{bx}^2}{l_{0L}^2 l_{0R}^2} + \gamma}{2 + \gamma l_{bx}^2} a_m^2\right) \right\}. \end{aligned} \quad (\text{B8})$$

A particularly interesting expression is the homogeneous field exchange coupling $J(\bar{B}, B_{dif} = 0)$ [13], which we list below (in addition to Eq. (14)) which is the inhomogeneous case $J(\bar{B} = 0, B_{dif})$). Since for this case $B_R = B_L$, we simplify our notation by using $l_0 = l_{0R/L}$ for the characteristic length. Also the overlap becomes $S(\bar{B}, B_{dif} = 0) = \exp(-(a_m/l_0)^2) \exp\left(-\left(\frac{1}{2}l_0 b a_m\right)^2\right)$.

$$\begin{aligned}
J(\overline{B}, B_{dif} = 0) = & \frac{2S^2}{1 - S^4} \left\{ \frac{\hbar^2 a_m^2}{ml_0^4} - \frac{1}{2} \frac{e^2 \overline{B}^2}{mc^2} a_m^2 \left(1 - \frac{1}{8} b^2 l_0^4 \right) - \frac{2V_0 l_x l_y}{\sqrt{(l_0^2 + l_x^2)(l_0^2 + l_y^2)}} \right. \\
& \times \left[\exp \left(-\frac{(a - a_m)^2}{l_0^2 + l_x^2} \right) + \exp \left(-\frac{(a + a_m)^2}{l_0^2 + l_x^2} \right) - 2 \exp \left(-\frac{a^2}{l_0^2 + l_x^2} + \frac{l_0^2 (bl_0 a_m)^2}{4(l_0^2 + l_y^2)} \right) \right] \\
& - \frac{2V_b l_{bx} l_{by}}{\sqrt{(l_0^2 + l_{bx}^2)(l_0^2 + l_{by}^2)}} \left[\exp \left(\frac{l_0^2 (bl_0 a_m)^2}{4(l_0^2 + l_{by}^2)} \right) - \exp \left(-\frac{a_m^2}{l_0^2 + l_{bx}^2} \right) \right] \\
& \left. - \sqrt{\frac{\pi}{2}} \frac{e^2}{\varepsilon l_0} e^{(\frac{1}{2} bl_0 a_m)^2} \left[I_0 \left(\left(\frac{1}{2} bl_0 a_m \right)^2 \right) - S I_0 \left(\left(\frac{a_m}{l_0} \right)^2 \right) \right] \right\}. \tag{B9}
\end{aligned}$$

- [1] R.P. Feynman, Int. J. Theor. Phys. **21**, 467 (1982); D. Deutsch, Proc. R. Soc. Lond. A **400**, 97 (1985).
- [2] P.W. Shor, in *Proceedings of the 35th Annual Symposium on the Foundations of Computer Science* (IEEE Press, Los Alamitos, CA), p. 124-133 (1994); L.K. Grover, Phys. Rev. Lett. **79**, 325 (1997).
- [3] P.W. Shor, Phys. Rev. A **52**, R2493 (1995); A. M. Steane, Phys. Rev. Lett. **77**, 793 (1996).
- [4] C.A. Sacket, D. Kielpinski, B.E. King, C. Langer, V. Meyer, C.J. Myatt, M. Rowe, Q.A. Turchette, W.M. Itano, D.J. Wineland, and C. Monroe, Nature **404**, 256 (2000).
- [5] L.M.K. Vandersypen, M. Steffen, G. Breyta, C.S. Yannoni, R. Cleve, and I.L. Chuang, Phys. Rev. Lett. **85**, 5452 (2000).
- [6] S.L. Braunstein, C.M. Caves, R. Jozsa, N. Linden, S. Popescu, and R. Schack, Phys. Rev. Lett. **83**, 1054 (1999).
- [7] B.E. Kane, Nature, **393**, 133 (1998); R. Vrijen, E. Yablonovitch, K. Wang, H.W. Jiang, A. Balandin, V. Roychowdhury, T. Mor, and D.P. Divincenzo, Phys. Rev. A **62**, 12306 (2000).
- [8] D. Loss and D.P. Divincenzo, Phys. Rev. A **57**, 120 (1998).
- [9] D.P. Divincenzo, Phys. Rev. A **51**, 1015 (1995).
- [10] G. Burkard, D. Loss, D.P. Divincenzo, and J.A. Smolin, Phys. Rev. B **60**, 11404 (1999).
- [11] X. Hu, R. de Sousa, and S. Das Sarma, Phys. Rev. Lett. **86**, 918 (2001).
- [12] D.P. Divincenzo, D. Bacon, J. Kempe, G. Burkard, and K.B. Whaley, Nature, **408**, 339 (2000); D. Bacon, J. Kempe, D.A. Lidar, and K.B. Whaley, Phys. Rev. Lett. **85**, 1758 (2000); D. Bacon, K.R. Brown, and K.B. Whaley, Preprint quant-ph/0012018.
- [13] G. Burkard, D. Loss, and D.P. Divincenzo, Phys. Rev. B **59**, 2070 (1999).
- [14] X. Hu and S. Das Sarma, Phys. Rev. A **61**, 62301 (2000).
- [15] I. Shavitt, in *Methods in Computational Physics* Vol 2, Academic Press, N.Y. (1963).
- [16] V. Fock, Z. Phys. **47**, 446 (1928); C. Darwin, Proc. Cambridge Philos. Soc. **27**, 86 (1930).

$\bar{B} = 0$ Tesla			
B_{dif} [Tesla]	$\sum_{n=1,2,3} \sum_m \frac{ \langle 00 \Delta H nm \rangle ^2}{ E_{00} - E_{nm} }$	$\sum_{n=2,3} \sum_m \frac{ \langle 00 \Delta H nm \rangle ^2}{ E_{00} - E_{nm} }$	$\sum_{n=3} \sum_m \frac{ \langle 00 \Delta H nm \rangle ^2}{ E_{00} - E_{nm} }$
0	0 meV	0 meV	0 meV
1	0.041	0.037	0.002
2	0.163	0.143	0.011
4	0.744	0.591	0.053
6	1.95	1.37	0.156

$\bar{B} = 4$ Tesla			
	0 meV	0 meV	0 meV
0	0 meV	0 meV	0 meV
1	0.038	0.034	0.002
2	0.153	0.141	0.009
4	0.694	0.603	0.041
6	1.91	1.49	0.142

TABLE I. Energy correction of the lowest Fock-Darwin state (S) when P, D and F levels are included in an inhomogeneous field calculation. ΔH contains all the inhomogeneous field terms that show up in the one particle Hamiltonian h_i (Eq. (17)). The quantum dot parameters (defined below Eq. (8)) are the same as the ones used in Figs. 2, 3 and 4.

n	m	Eigenstate
0	0	$\frac{1}{\sqrt{\pi l_0^2}} e^{-\frac{r^2}{2l_0^2}}$
1	1	$\frac{1}{\sqrt{\pi l_0^2}} r e^{-\frac{r^2}{2l_0^2}} e^{i\theta}$
2	0	$\frac{1}{\sqrt{\pi l_0}} (1 - \frac{r^2}{l_0^2}) e^{-\frac{r^2}{2l_0^2}}$
2	2	$\frac{1}{\sqrt{2\pi l_0^3}} r^2 e^{-\frac{r^2}{2l_0^2}} e^{2i\theta}$

TABLE II. S, P and D Fock-Darwin energy eigenstates for positive magnetic quantum number m. For negative m, complex conjugate the corresponding wave function.

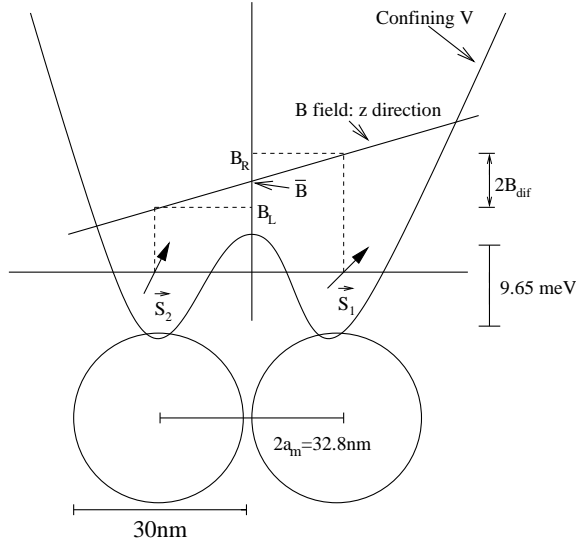


FIG. 1. Confining potential (defined in Eq. (8) of the text) that models the double dot structure we study. The magnetic field profile is such that the difference between the fields on the right and left is $2B_{dif}$ and the average $\bar{B} = (B_R + B_L)/2$ is in the midpoint between the dots. The quantum dot parameters for all the calculations in this paper are given in the text following Eq. (8).

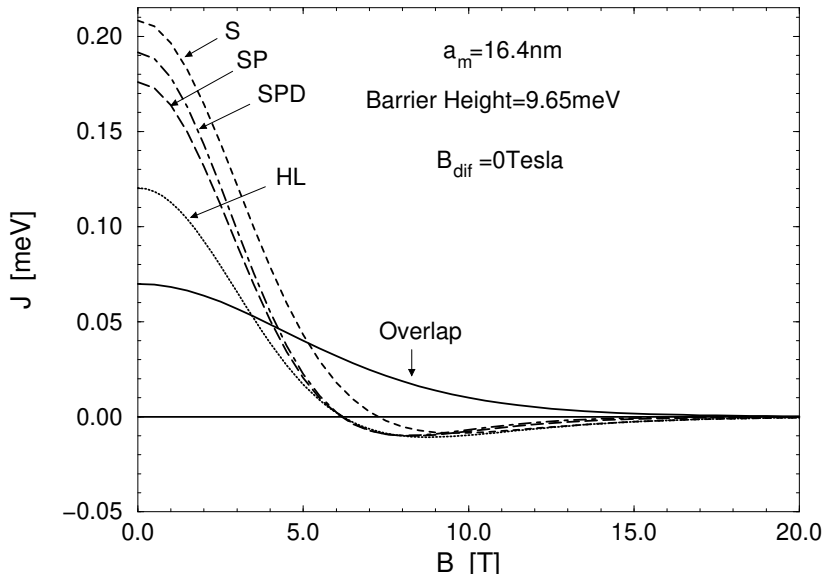


FIG. 2. Exchange energy J of the coupled dots in a homogeneous magnetic field B . The molecular orbital approximations (S, SP, SPD) are very close to each other and represent a quantitative improvement over the simpler Heitler-London (HL). Note that J is plotted in the unit of meV, while the overlap S is dimensionless. The analytical formula for the HL theory are given in Appendix B.

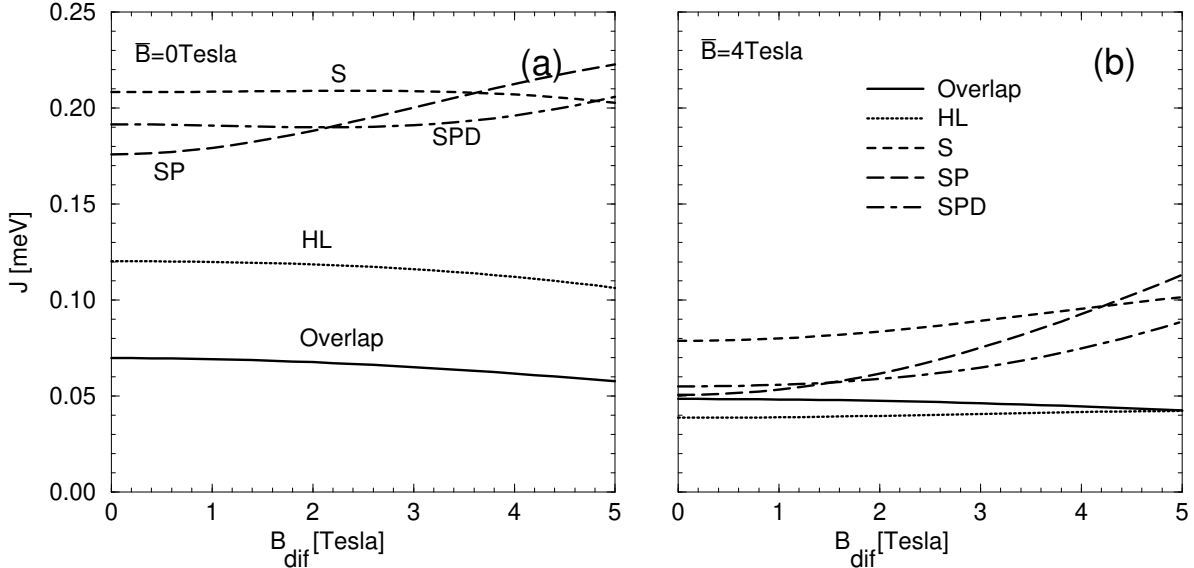


FIG. 3. Exchange energy J of the double dot structure when an inhomogeneous magnetic field is present with average $\bar{B} = (B_R + B_L)/2$ equal to 0 (Fig. 3a) and 4 (Fig. 3b) Tesla respectively. $B_{dif} = (B_R - B_L)/2$ is half the difference between the fields at the center of each dot.

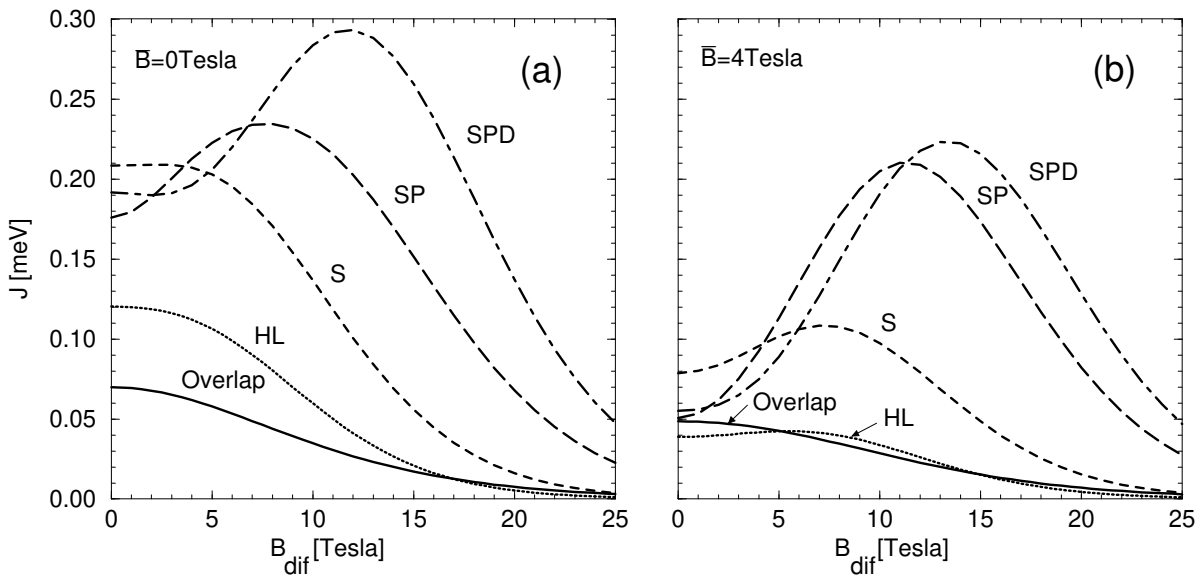


FIG. 4. Exchange energy J of the double dot when an inhomogeneous magnetic field is present with average \bar{B} equal to 0 (Fig. 4a) and 4 (Fig. 4b) Tesla respectively. For completeness, we show J as a function of B_{dif} up to 25 T, which is much higher than what can be obtained in the laboratory.